Cavity-assisted thermometry for a single trapped ion

Ding Fang,[1,2,4,*] Wei-Bin Chen,[1,2,4,*] Cheng-Hao Zhang,[1,2,4] Jin-Ming Cui,[1,2,3,4,†] Yun-Feng Huang,[1,2,3,4,‡] Chuan-Feng Li,[1,2,3,4] and Guang-Can Guo[1,2,3,4]

[1] *Laboratory of Quantum Information, University of Science and Technology of China, Hefei 230026, China*

[2] *Anhui Province Key Laboratory of Quantum Network, University of Science and Technology of China, Hefei 230026, China*

[3] *CAS Center for Excellence in Quantum Information and Quantum Physics, University of Science and Technology of China, Hefei 230026, China*

[4] *Hefei National Laboratory, University of Science and Technology of China, Hefei 230088, China*

(Received 16 May 2025; revised 2 July 2025; accepted 14 July 2025; published 14 August 2025)

We propose and demonstrate two cavity-assisted thermometry methods that exploit the sensitivity of cavity radiation to the position of the ion in the cavity mode to achieve highly sensitive temperature measurements. Our analysis allows us to determine the relative positions of the rf null and the cavity mode by the change of cavity emission at different positions of the ion in the cavity mode. By analyzing the second-order correlation function of the cavity emission, temperature measurements from near the motional ground state to over tens of millikelvin can be achieved and motion patterns of different frequencies can be characterized. We demonstrate our approach by measuring the temperature of a single $^{138}Ba^{+}$ ion trapped in a fiber microcavity with a length of 230 μm using both proposed methods, achieving comparable results.

DOI: 10.1103/vjl6-crbg

I. INTRODUCTION

Optical cavities are efficient quantum interfaces that enhance the interaction between matter and light [1–3]. Microcavities reduce the mode volume, thereby strengthening light-matter coupling strength g and cooperativity C, which are essential for realizing practical quantum networks. These microcavities have been integrated into a variety of quantum systems [4–7]. Trapped ions are particularly promising as quantum information carriers due to their long coherence times and high-fidelity gate operations. They have been coupled to optical cavities, enabling demonstrations of small-scale quantum networks [8–11]. Recent progress has also been made in trapped ion-microcavity systems [12–18]. In these systems, minimizing temperature is critical, as thermal motion impacts coupling strength, gate fidelity, and coherence time. Accurate thermometry plays a crucial role in evaluating cooling mechanisms, diagnosing heating sources, and optimizing experimental conditions.

However, the presence of optical microcavities makes some existing temperature measurement methods ineffective or more complicated. Existing temperature measurement methods cover different temperature ranges. For regions near the motional ground state, methods such as the time evolution of red or blue sideband processes [19], the blue-to-red sideband ratio method [20–22], and carrier Rabi spectroscopy have been employed to accurately determine temperature [20]. The bichromatic driving method [23], singular value decomposition frequency-domain analysis [24], and rapid adiabatic passage (RAP) enable researchers not only to measure ion temperature but also to probe velocity distributions in the system [25–27]. However, these methods are generally limited to low temperatures and require quantum state-detection capabilities. In ion-microcavity systems, dielectric cavity mirrors can cause significant heating of the ion [28]. Therefore, the temperature when the ion reaches thermal equilibrium is likely to exceed the measurement range of these methods. In temperature regimes exceeding 1 mK, spatial thermometry methods [29–31] provide straightforward means of temperature measurement. By directly fitting the size of ion images, temperature can be determined. However, the accuracy of this method depends on the point spread function of the imaging system, imposing high requirements on the imaging system. When the phonon frequency reaches the megahertz regime due to a tight trapping potential, objective-lens systems in typical ion trap setups may lack the resolution required for effective thermometry. Another type of thermometry utilizes the Doppler effect of the ion in motion. Doppler recooling technique utilizes fluorescence intensity changes during ion cooling to

*These authors contributed equally to this work.
†Contact author: jmcui@ustc.edu.cn
‡Contact author: hyf@ustc.edu.cn

 © 2025 American Physical Society

determine ion temperature [32,33]. This method is typically applicable for average phonon numbers $\bar{n} > 10^4$. Similarly, linewidth measurement methods can also only be used for high-temperature measurements due to the large upper-level radiation linewidth (approximately $2\pi \times 20$ MHz) used in cooling cycles [34–36]. Dark resonance thermometry [37–39] overcomes the above limitations. However, this method relies on accurate assessment of laser Rabi frequencies and requires complex simulations, calculations and data fitting. Since the cavity affects the radiation linewidth, all these temperature measurement methods using the Doppler effect must consider the influence of the resonant cavity when applied to cavity QED systems, requiring accurate measurement of the coupling strength between the matter and the cavity. Additionally, there are other temperature measurement methods with special requirements, such as deep neural-network-based thermometry [40] and spin-dependent kick methods using mode-locked lasers [41].

Here we analyze how ion motion affects cavity emission and demonstrate two cavity-assisted temperature measurement methods. By analyzing the second-order correlation function of photons collected by the cavity, temperature measurement capabilities ranging from near the motional ground state to over tens of millikelvin can be achieved, and various ion-motion modes with different frequencies can be resolved. These methods exploit the positional sensitivity of the fluorescence of the ion in the cavity mode and offer sensitivity that far exceeds that of spatial thermometry methods using objective lens imaging [42,43]. These temperature measurement methods are insensitive to excitation laser parameters, do not require assessment of cavity-ion coupling strength, and do not require qubit preparation, control or detection capabilities.

II. THEORY

Consider the one-dimensional motion of an ion in a Paul trap along the cavity axis. The ion's motion can be expressed using the solution of the Mathieu equation:

$$\hat{x}(t) = x_0\left[1 - \frac{q}{2}\sin(\omega_{\rm rf}t)\right] + \sqrt{\frac{\hbar}{2m\omega_p}}\left[1 - \frac{q}{2}\sin(\omega_{\rm rf}t)\right]\left(\hat{a}e^{-i\omega_p t} + \hat{a}^\dagger e^{i\omega_p t}\right). \tag{1}$$

Here, x_0 represents the ion's static offset from the rf null, ω_p is the phonon motion frequency, $\omega_{\rm rf}$ is the rf drive frequency in the Paul trap, m is the ion mass, $\hbar$ is the reduced Planck constant and q is a parameter related to the potential well's shape, known as the secular parameter.

Assuming the ion is coupled to an optical cavity not under the strong coupling regime, fluorescence collected by the cavity can be considered approximately proportional to the square of coupling strength $g^2(x)$ (corrections may be required in the strong coupling regime) [2]. As shown in Fig. 1, the fluorescence collected by the cavity varies with the ion's position relative to the cavity mode. In the symmetric cavity center region, which is much smaller than the cavity length, the coupling strength variation along the cavity direction approximates the electric-field distribution of a one-dimensional standing-wave field, $g(x) \propto \cos(kx)$, where k is the wave number of the on-resonance wavelength. The fluorescence collected in the cavity can be expressed as

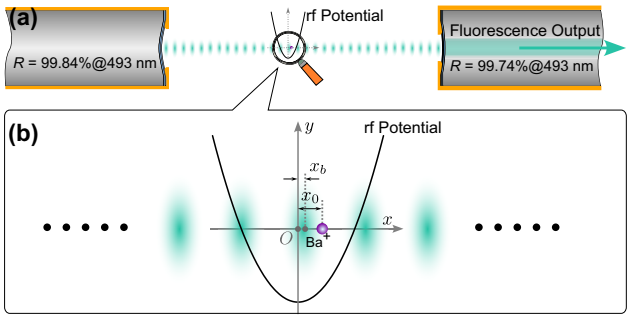

FIG. 1. An ion oscillates in the cavity mode under the rf potential $U(x)$ of a Paul trap. In the figure, the rf null is taken as the coordinate origin. The position x_0 represents the ion's location, while x_b denotes the position of the nearest antinode of the cavity mode.

$$\hat{I}(t) \propto \cos^2(k(\hat{x}(t) - x_b)). \tag{2}$$

Here, x_b represents the deviation of the cavity antinode from the rf null.

A thermal state density operator can be decomposed on coherent-states basis like

$$\hat{\rho}_{\rm th} = \int {\rm d}^2\alpha\, P_{\rm th}(\alpha)\,|\alpha\rangle\,\langle\alpha|\,, \tag{3}$$

where

$$P_{\rm th}(\alpha) = \frac{1}{\pi\bar{n}}\exp\left(-\frac{|\alpha|^2}{\bar{n}}\right). \tag{4}$$

Here, $\bar{n}$ represents the average phonon number, which is related to temperature T by

$$T = \frac{\hbar\omega_p}{k_B \ln\left(\frac{\bar{n}+1}{\bar{n}}\right)}, \tag{5}$$

where k_B is the Boltzmann constant. Then the fluorescence collected by the cavity for an ion in a thermal state is

$$\langle I(t)\rangle_{\rm th} \propto {\rm Tr}[\hat{\rho}_{\rm th}\hat{I}(t)] \propto \int {\rm d}^2\alpha\, P_{\rm th}(\alpha)\,\langle\alpha|\,\hat{I}(t)\,|\alpha\rangle\,. \tag{6}$$

Under the first-order approximation, the averaged fluorescence intensity can be expressed as

$$\langle \bar{I} \rangle_{\text{th}} \propto 1 + \exp\left[-\frac{\eta^2}{2}(2\bar{n}+1)\left(1+\frac{q^2}{8}\right)\right] \times J_0\big(k\,x_0\,q\big)\, I_0\left(\frac{1}{2}\,\eta^2\,\bar{n}\,q\sqrt{1+\frac{q^2}{16}}\right) \times \cos\big[\,2k\,(x_0 - x_b)\big], \tag{7}$$

where $\eta = k\sqrt{2\hbar/m\omega_p}$ is the Lamb-Dicke parameter, J_0 is the zeroth-order Bessel function of the first kind and I_0 denotes the zeroth-order modified Bessel function of the first kind. This equation reflects the fluctuations of fluorescence emitted by an ion trapped in a Paul trap when moving along the cavity direction. When the ion's temperature rises, the vibration amplitude grows. The averaged fluorescence intensity at the cavity antinode decreases, while that at the node goes up. We define the intensity ratio as $R = ((\langle \bar{I} \rangle_{\text{th,min}})/(\langle \bar{I} \rangle_{\text{th,max}}))$, which rises as the temperature increases. Further, as the ion's position within the cavity mode varies with time, the fluorescence intensity collected in the cavity also changes. This variation is reflected in the second-order correlation function of the emitted photons, which exhibits periodic fluctuations related to the ion's motion frequency. This method not only allows us to measure the ion's temperature without physically moving it but also enables the characterization of different ion motions, such as micromotion.

The second-order correlation function of the photons collected from the cavity can be expressed as

$$g^{(2)}(\tau) = \frac{\langle \langle I(t) \rangle_{\text{th}} \langle I(t-\tau) \rangle_{\text{th}} \rangle_t}{\langle \langle I(t) \rangle_{\text{th}} \rangle_t^2}. \tag{8}$$

By performing a Fourier transform, the spectral information can be extracted

$$F(\omega) = \int_{-\infty}^{\infty} g^{(2)}(\tau) e^{-i\omega\tau}\, \mathrm{d}\tau. \tag{9}$$

We then observe the spectral height of the phonon frequency-related term, denoted as F_{ω_p}. Within a certain range, the height of this spectral term increases with temperature and enters a decreasing region beyond. While Eq. (7) provides an analytical expression for R under a first-order approximation, its accuracy can be limited, especially at higher temperatures. To obtain accurate numerical results for comparison with experimental data, we employed a Monte Carlo algorithm to simulate the decomposition of the thermal state in the coherent-state basis. This simulation allows for a precise calculation of the temperature dependence of both the intensity ratio R and the spectral height F_{ω_p}.

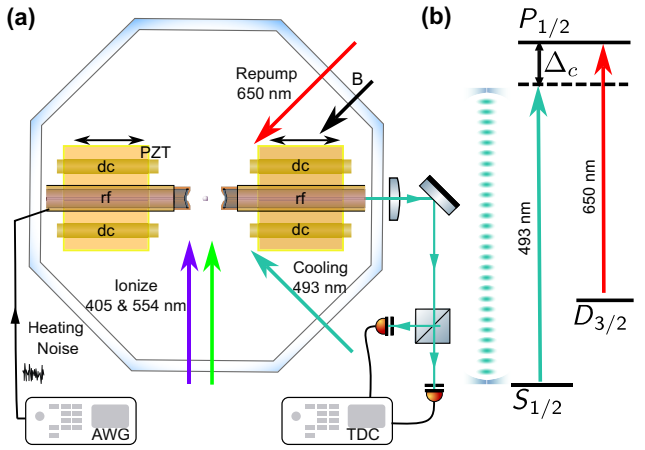

FIG. 2. (a) A single $^{138}Ba^+$ ion is trapped between two electrodes with cavity mirrors on their ends, while other regions are gold coated. The ion is Doppler cooled, and fluorescence collected from the cavity is split into two paths to measure the second-order correlation function. White noise applied to the rf electrodes is used to heat the ion. (b) Energy-level diagram of $^{138}Ba^+$. Doppler cooling is performed using the 493-nm laser, the 650-nm laser is used for repump, and the cavity is on resonance with the 493-nm driving laser.

III. EXPERIMENTS

A single $^{138}Ba^+$ ion is trapped in the apparatus shown in Fig. 2(a). Several electrodes form a needle trap, with the yellow-labeled central two electrodes providing the rf voltage required for ion trapping, and the four side electrodes providing dc voltage to compensate for micromotion. The ion is trapped between the rf electrodes, which have an approximate diameter of 270 μm. The central rf electrode is machined from a gold-coated fiber with a concave mirror on the end surface of a radius of curvature of approximately 300 μm and coated with high-reflectivity coating. The two central electrodes form an optical cavity, and the ion is trapped in the cavity mode. The cavity emission is collected through the fiber integrated into the rf electrode.

The ion is Doppler cooled in the cavity using a red-detuned 493-nm laser. A 650-nm laser is used for repumping. Using a bias T to superimpose a dc offset on one of the rf electrodes to move the ion along the cavity axis. The cavity length was tuned via a piezoelectric ceramic beneath the electrode and locked to resonance with the cooling laser. As shown in Fig. 2(b), the cavity length is approximately 230 μm, with a beam waist radius of about 5 μm and a decay rate of $\kappa = 2\pi \times 200$ MHz. The cooperative factor $C \approx 0.3$, placing it in the weak coupling regime.

During the continuous Doppler cooling process, the 493-nm fluorescence emitted by the ion is collected by the cavity. A nonpolarizing beam splitter (NPBS) divides the fluorescence into two beams, which enter two photomultiplier tubes (PMTs) to facilitate measurement of the second-order correlation function.

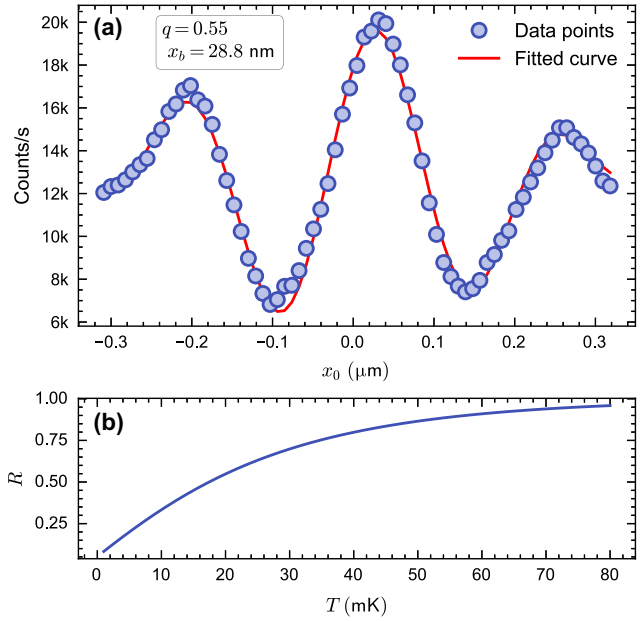

FIG. 3. (a) Cavity emission variation as the ion's position is scanned along the cavity axis, with the red curve being a fit to the calculation result. (b) The numerically calculated intensity ratio of cavity emission R, as a function of temperature T.

As shown in Fig. 3(a), the fluorescence intensity changes as the ion moving along the cavity axis deviates from a cosine profile due to micromotion, while the observed asymmetry arises from a displacement between the rf null and the cavity antinode. Fitting according to Eq. (7) yields the secular parameter q and the deviation x_b of the rf null from the cavity antinode. The ratio R of the intensity at the node and antinode can reflect the ion's temperature. Figure 3(b) shows the numerical calculation result of the relationship between the intensity ratio R and temperature T under the fitted parameters. As the temperature of the ion rises, its motion amplitude increases accordingly, leading to a rise in the intensity ratio. This approach enables us to rapidly ascertain the ion's temperature.

Measuring the second-order correlation function of cavity emission can provide more information on ion motion. As shown in Fig. 2(a), the Hanbury Brown-Twiss (HBT) measurement setup splits cavity-collected photons into two paths using a NPBS, and a time-digital converter (TDC) records photon arrival time to obtain the second-order correlation function.

Figures 4(a) and 4(e), respectively, show the second-order correlation function when the ion locates halfway between the antinode and node of the cavity mode and when it is near the antinode. The $g^{(2)}(\tau)$ approaching 0 at $\tau = 0$ indicates that the system is an ideal single-photon source. Subsequently, the periodic fluctuations in the second-order correlation function are caused by the ion's motion in the cavity mode. As shown in Fig. 4(c), when the ion is between the node and antinode of the cavity mode, the fluctuations mainly manifest at the phonon frequency. The data reveals an ion secular motion frequency of 2.85 MHz along the cavity direction with a signal-to-noise ratio (SNR) of approximately 50 dB. When the ion is near the antinode, as shown in Fig. 4(h), the fluctuations mainly manifest at twice the phonon frequency. The frequency content of the fluorescence signal, shown in Fig. 4, depends directly on the ion's equilibrium position within the standing wave. When the ion oscillates on a slope of the electric-field strength profile, its brightness variation directly tracks its mechanical motion, resulting in a spectral peak at the phonon frequency ω_p. However, when the ion oscillates around an antinode—a point of maximum brightness—the intensity decreases regardless of the direction the ion moves. This causes the fluorescence intensity to undergo two full modulation cycles for every single mechanical oscillation. As a result, the dominant frequency in the correlation signal becomes twice the phonon frequency, shifting the spectral peak to $2\omega_p$, as observed when comparing Figs. 4(d) and 4(h). Additionally, since the ion has deviated from the rf null, a peak corresponding to the micromotion frequency of $\omega_{\mathrm{rf}} = 19.906$ MHz also appears in the spectrum. Motions of different frequencies can be easily distinguished in the spectrum of the second-order correlation function.

To change the ion's temperature, we applied white electrical noise to the rf electrode using an arbitrary waveform generator (AWG). This causes random displacement of the trap potential while keeping the trap frequency constant. Combined with the dissipative process of laser cooling, a steady state with adjustable temperature T can be reached after a duration of $t \geq$ 2 ms. The temperature is regulated by the electric-field noise amplitude, where the temperature T is proportional to the square of the root-mean-square voltage V of the white electrical noise ($T \propto V^2$), simulating an equivalent thermal bath for the trapped ion [38]. Figure 5(a) shows the variation in spectral height at the phonon frequency as the temperature increases due to amplified white-noise driving. Due to the nonmonotonic temperature dependence of spectral height, an accurate ion temperature can be obtained by either: (1) using the intensity ratio method to roughly determine the temperature first; or (2) heating the ion with the described technique and analyzing the monotonicity of the spectral height-voltage curve to judge if the actual temperature is below or above the peak temperature of the simulation curve.

The sensitivity of the correlation-based thermometry method is governed by the SNR of the second-order correlation function $g^{(2)}(\tau)$. In our experiment, we achieved a measured SNR of $\mathrm{SNR}_{\mathrm{meas}} = 50$ dB at a temperature of $T_{\mathrm{meas}} = 6$ mK.

At low temperatures, the amplitude of fluorescence modulation is approximately proportional to the ion's

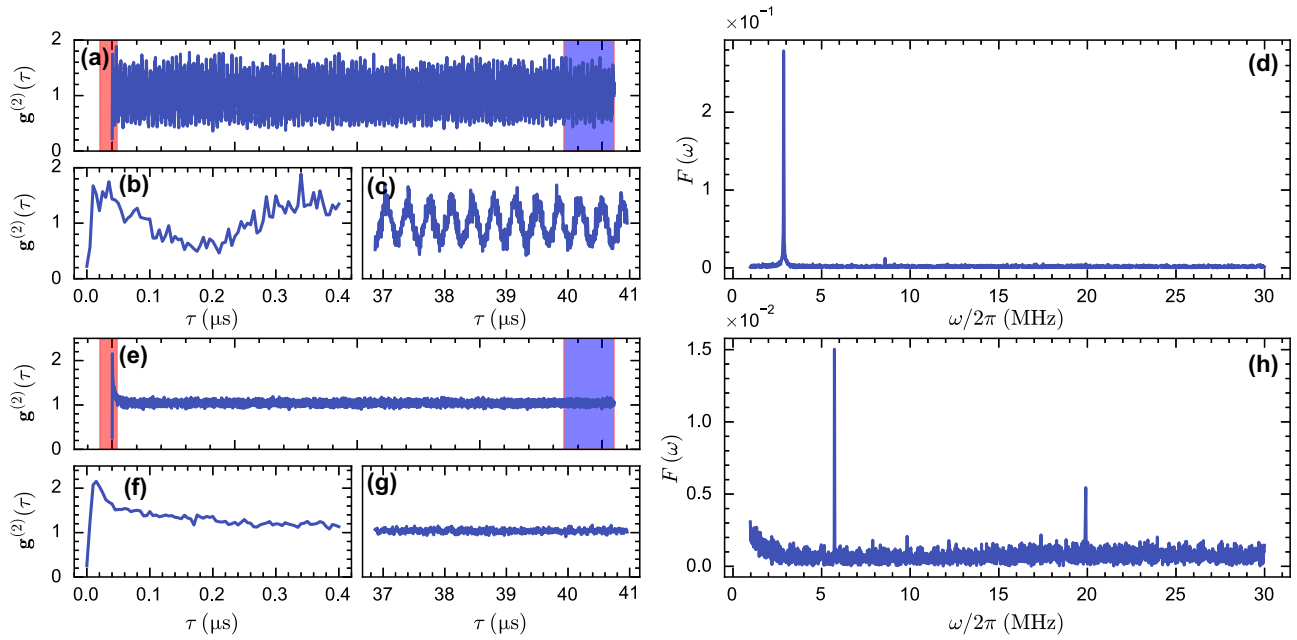

FIG. 4. (a) The second-order correlation function of fluorescence collected by the cavity when the ion locates between the cavity antinode and node. (b),(c) Local magnification of the second-order correlation function. (d) The spectrum of the second-order correlation function directly reflects the ion's motion (initial rising segment subtracted prior to spectral analysis), with a SNR of 50 dB achieved in a photon collection time of 20 s. (e) The second-order correlation function when the ion locates near the antinode. (f),(g) Local magnification of the second-order correlation function. (h) The peak of the spectrum shifts to twice the phonon frequency. Due to the increased position offset from the rf null, a peak corresponding to the micromotion frequency can be observed in the spectrum.

motional amplitude, which scales as $\sqrt{T}$. Since the SNR scales linearly with the modulation depth and with the square root of the total number of detected photons N, we have the proportionality

$$\mathrm{SNR} \propto T \cdot \sqrt{N}. \tag{10}$$

Assuming the total photon count N remains constant (longer integration time compensates for reduced photon rates at lower temperatures), the minimum detectable temperature $T_{\min}$ under a conservative threshold of $\mathrm{SNR}_{\min} = 5$ dB can be estimated as

$$T_{\min} \approx T_{\mathrm{meas}} \times 10^{(\mathrm{SNR}_{\min} - \mathrm{SNR}_{\mathrm{meas}})/20}, \tag{11}$$

which yields $T_{\min} \approx 20$ μK. This suggests that the correlation-based thermometry method is capable of detecting temperatures near the motional ground state, with ultimate sensitivity limited by photon collection efficiency, residual heating, and stability of ion's offset. Since this method is based on position measurement, the phonon frequency ω_p critically affects the measurement sensitivity. This relationship can be quantified by modeling the ion as a harmonic oscillator in thermal equilibrium at temperature T. The ion's motional amplitude A is related to its thermal energy by $A \approx \sqrt{2k_B T/(m\omega_p^2)}$. This shows that for a given temperature, the amplitude scales inversely with the phonon frequency, i.e., $A \propto 1/\omega_p$. A smaller amplitude at higher phonon frequencies leads to a weaker fluorescence modulation signal at low temperature, thus reducing the thermometry sensitivity. Consequently, the measurement sensitivity is improved at lower phonon frequencies. Figure 5(b) presents the variation in spectral height as the cooling light detuning is scanned. It displays the synchronous change in intensity ratio with detuning of cooling laser. Both temperature measurement methods show that the cooling effect is better when the cooling laser detuning is between −15 and −20 MHz. Figure 5(c) shows the relationship between the temperature obtained from the data in (b) and the detuning of the cooling light. The temperature measurement results of the two methods are relatively close. The higher temperature measured by the intensity ratio method may be due to the drift of the electrical noise intensity in the experimental system. In addition, the intensity ratio method moves the ion away from the rf null, which may also weaken the cooling effect.

IV. CONCLUSION

We have demonstrated two cavity-assisted thermometry methods suitable for trapped ions in cavity QED systems. The spatial fluorescence method provides a quick estimate of ion temperature, while the photon correlation method offers high sensitivity and resolves distinct motional components, including micromotion. Compared

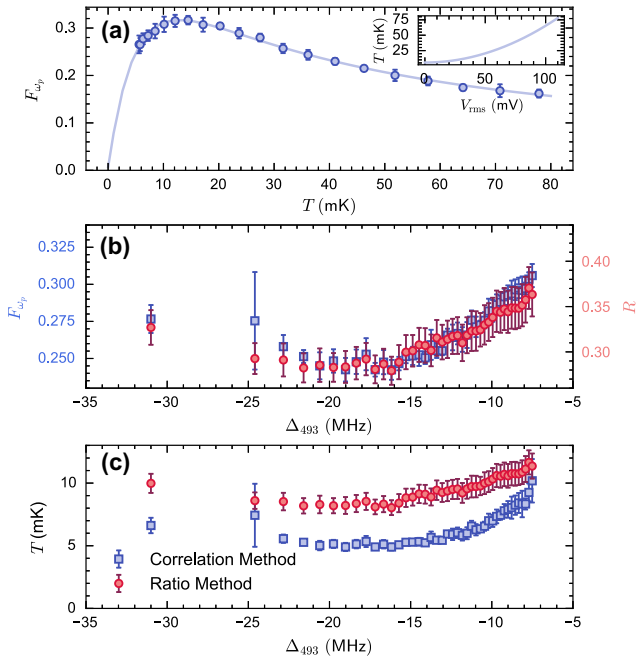

FIG. 5. (a) The spectral height at the phonon frequency as a function of temperature. White noise applied to the rf electrode heats the ion. The inset in the top right shows the relationship between the effective temperature and the white noise voltage obtained from fits, this curve is derived by mapping the measured F_{ω_p} values at different noise voltages to their corresponding temperatures via the simulated curve. As we are currently unable to cool the ion to lower temperatures in our system, the lowest measured temperature shown in the figure is about 6 mK. (b) Scanning the cooling light detuning, the blue data points show the spectral height at the phonon frequency as a function of detuning. The red data shows the ratio of minimum to maximum intensity R as a function of cooling laser detuning when scanning the ion's position. (c) Temperature measurement results corresponding to the data in (b).

to existing techniques, our proposed cavity-assisted thermometry demonstrates significant advantages in several key aspects. It does not require complex quantum state preparation or detection, making it operationally simpler than methods relying on sideband ratios or carrier Rabi oscillations, and it can cover a broader temperature range. Furthermore, the method can effectively probe low-temperature regimes that are challenging for traditional Doppler spectroscopy, while its results are not dependent on a precise assessment of laser and cavity parameters, which is a key practical advantage in cavity QED systems. In comparison with spatial imaging thermometry, our method utilizes the intracavity standing wave for position detection, offering a spatial resolution far exceeding that of a conventional objective lens system. This high resolution greatly enhances the detection sensitivity of the ion's motion. Consequently, our method remains effective for temperature measurement even in cases where the phonon frequency is high and the ion's motional amplitude is correspondingly small.

Our results expand the thermometry toolbox for trapped-ion experiments and offer practical tools for diagnosing and optimizing cavity-integrated quantum network nodes. In future work, these methods can be generalized to multi-ion systems, enabling position-dependent thermometry of collective ion motion and local heating dynamics. Incorporating the influence of the Doppler effect in numerical calculations will allow the temperature measurement range of this method to be extended to higher temperatures.

ACKNOWLEDGMENTS

This work was supported by the National Key Research and Development Program of China (2024YFA1409403), the National Natural Science Foundation of China (Grants No. 11734015, and No. 12204455), the Innovation Program for Quantum Science and Technology (Grant No. 2021ZD0301604 and No. 2021ZD0301200) and the Key Research Program of Frontier Sciences, CAS (Grant No. QYZDY-SSWSLH003).

DATA AVAILABILITY

The data that support the findings of this article are openly available [44].

[1] L.-M. Duan and C. Monroe, Colloquium: Quantum networks with trapped ions, Rev. Mod. Phys. **82**, 1209 (2010).
[2] A. Reiserer and G. Rempe, Cavity-based quantum networks with single atoms and optical photons, Rev. Mod. Phys. **87**, 1379 (2015).
[3] A. Reiserer, Colloquium: Cavity-enhanced quantum network nodes, Rev. Mod. Phys. **94**, 041003 (2022).
[4] J. Wang, X.-L. Zhou, Z.-M. Shen, D.-Y. Huang, S.-J. He, Q.-Y. Huang, Y.-J. Liu, C.-F. Li, and G.-C. Guo, Purcell-enhanced generation of photonic Bell states via the inelastic scattering off single atoms, Phys. Rev. Lett. **134**, 053401 (2025).
[5] J. Wang, D.-Y. Huang, X.-L. Zhou, Z.-M. Shen, S.-J. He, Q.-Y. Huang, Y.-J. Liu, C.-F. Li, and G.-C. Guo, Ultrafast high-fidelity state readout of single neutral atom, Phys. Rev. Lett. **134**, 240802 (2025).
[6] D. Niemietz, P. Farrera, S. Langenfeld, and G. Rempe, Nondestructive detection of photonic qubits, Nature **591**, 570 (2021).
[7] R. Albrecht, A. Bommer, C. Deutsch, J. Reichel, and C. Becher, Coupling of a single nitrogen-vacancy center in diamond to a fiber-based microcavity, Phys. Rev. Lett. **110**, 243602 (2013).
[8] V. Krutyanskiy, M. Canteri, M. Meraner, J. Bate, V. Krcmarsky, J. Schupp, N. Sangouard, and B. P. Lanyon, Telecom-wavelength quantum repeater node based on a trapped-ion processor, Phys. Rev. Lett. **130**, 213601 (2023).

[9] M. Keller, B. Lange, K. Hayasaka, W. Lange, and H. Walther, A calcium ion in a cavity as a controlled single-photon source, New J. Phys. **6**, 95 (2004).

[10] A. Stute, B. Casabone, P. Schindler, T. Monz, P. O. Schmidt, B. Brandstätter, T. E. Northup, and R. Blatt, Tunable ion–photon entanglement in an optical cavity, Nature **485**, 482 (2012).

[11] B. Casabone, A. Stute, K. Friebe, B. Brandstätter, K. Schüppert, R. Blatt, and T. E. Northup, Heralded entanglement of two ions in an optical cavity, Phys. Rev. Lett. **111**, 100505 (2013).

[12] S. Gao, J. A. Blackmore, W. J. Hughes, T. H. Doherty, and J. F. Goodwin, Optimization of scalable ion-cavity interfaces for quantum photonic networks, Phys. Rev. Appl. **19**, 014033 (2023).

[13] M. Teller, V. Messerer, K. Schüppert, K. Zou, D. A. Fioretto, M. Galli, P. C. Holz, J. Reichel, and T. E. Northup, Integrating a fiber cavity into a wheel trap for strong ion–cavity coupling, AVS Quantum Sci. **5**, 014701 (2023).

[14] B. Brandstätter, A. McClung, K. Schüppert, B. Casabone, K. Friebe, A. Stute, A. Schmidt, C. Deutsch, J. Reichel, R. Blatt *et al.*, Integrated fiber-mirror ion trap for strong ion-cavity coupling, Rev. Sci. Instrum. **84**, 123105 (2013).

[15] M. Steiner, H. M. Meyer, C. Deutsch, J. Reichel, and M. Köhl, Single ion coupled to an optical fiber cavity, Phys. Rev. Lett. **110**, 043003 (2013).

[16] T. G. Ballance, H. M. Meyer, P. Kobel, K. Ott, J. Reichel, and M. Köhl, Cavity-induced backaction in Purcell-enhanced photon emission of a single ion in an ultraviolet fiber cavity, Phys. Rev. A **95**, 033812 (2017).

[17] H. Takahashi, E. Kassa, C. Christoforou, and M. Keller, Cavity-induced anticorrelated photon-emission rates of a single ion, Phys. Rev. A **96**, 023824 (2017).

[18] H. Takahashi, E. Kassa, C. Christoforou, and M. Keller, Strong coupling of a single ion to an optical cavity, Phys. Rev. Lett. **124**, 013602 (2020).

[19] K. K. Mehta, C. D. Bruzewicz, R. McConnell, R. J. Ram, J. M. Sage, and J. Chiaverini, Integrated optical addressing of an ion qubit, Nat. Nanotechnol. **11**, 1066 (2016).

[20] D. Leibfried, R. Blatt, C. Monroe, and D. Wineland, Quantum dynamics of single trapped ions, Rev. Mod. Phys. **75**, 281 (2003).

[21] F. Diedrich, J. C. Bergquist, W. M. Itano, and D. J. Wineland, Laser cooling to the zero-point energy of motion, Phys. Rev. Lett. **62**, 403 (1989).

[22] C. Monroe, D. M. Meekhof, B. E. King, S. R. Jefferts, W. M. Itano, D. J. Wineland, and P. Gould, Resolved-sideband Raman cooling of a bound atom to the 3D zero-point energy, Phys. Rev. Lett. **75**, 4011 (1995).

[23] X. Q. Li, Y. Tao, T. Chen, W. Wu, Y. Xie, C. W. Wu, and P. X. Chen, Thermometry of trapped ions based on bichromatic driving, Phys. Rev. Appl. **22**, 064022 (2024).

[24] D. M. Meekhof, C. Monroe, B. E. King, W. M. Itano, and D. J. Wineland, Generation of nonclassical motional states of a trapped atom, Phys. Rev. Lett. **76**, 1796 (1996).

[25] A. V. Kirkova, W. Li, and P. A. Ivanov, Adiabatic sensing technique for optimal temperature estimation using trapped ions, Phys. Rev. Res. **3**, 013244 (2021).

[26] P. Mahmoudi, A. Ritboon, and R. Filip, Optimal quantum sensing of the nonlinear bosonic interactions using Fock states, Phys. Rev. Res. **6**, 043215 (2024).

[27] S. An, J. N. Zhang, M. Um, D. S. Lv, Y. Lu, J. H. Zhang, J. Yin, H. T. Quan, and K. Kim, Experimental test of the quantum Jarzynski equality with a trapped-ion system, Nat. Phys. **11**, 193 (2015).

[28] M. Teller, D. A. Fioretto, P. C. Holz, P. Schindler, V. Messerer, K. Schüppert, K. Zou, R. Blatt, J. Chiaverini, J. Sage *et al.*, Heating of a trapped ion induced by dielectric materials, Phys. Rev. Lett. **126**, 230505 (2021).

[29] B. Srivathsan, M. Fischer, L. Alber, M. Weber, M. Sondermann, and G. Leuchs, Measuring the temperature and heating rate of a single ion by imaging, New J. Phys. **21**, 113014 (2019).

[30] B. G. Norton, E. W. Streed, M. J. Petrasiunas, A. Jechow, and D. Kielpinski, Millikelvin spatial thermometry of trapped ions, New J. Phys. **13**, 113022 (2011).

[31] S. Knünz, M. Herrmann, V. Batteiger, G. Saathoff, T. W. Hänsch, and T. Udem, Sub-millikelvin spatial thermometry of a single Doppler-cooled ion in a Paul trap, Phys. Rev. A **85**, 023427 (2012).

[32] J. H. Wesenberg, R. J. Epstein, D. Leibfried, R. B. Blakestad, J. Britton, J. P. Home, W. M. Itano, J. D. Jost, E. Knill, C. Langer *et al.*, Fluorescence during Doppler cooling of a single trapped atom, Phys. Rev. A **76**, 053416 (2007).

[33] R. J. Epstein, S. Seidelin, D. Leibfried, J. H. Wesenberg, J. J. Bollinger, J. M. Amini, R. B. Blakestad, J. Britton, J. P. Home, W. M. Itano *et al.*, Simplified motional heating rate measurements of trapped ions, Phys. Rev. A **76**, 033411 (2007).

[34] T. Sikorsky, Z. Meir, N. Akerman, R. Ben-Shlomi, and R. Ozeri, Doppler cooling thermometry of a multilevel ion in the presence of micromotion, Phys. Rev. A **96**, 012519 (2017).

[35] W. Nagourney, G. Janik, and H. Dehmelt, Linewidth of single laser-cooled $^{24}Mg^{+}$ ion in radiofrequency trap, Proc. Natl. Acad. Sci. **80**, 643 (1983).

[36] M. Herrmann, V. Batteiger, S. Knünz, G. Saathoff, T. Udem, and T. W. Hänsch, Frequency metrology on single trapped ions in the weak binding limit: the $^{3}s_{1/2}$–$^{3}p_{3/2}$ transition in $^{24}Mg^{+}$, Phys. Rev. Lett. **102**, 013006 (2009).

[37] V. Tugayé, J.-P. Likforman, S. Guibal, and L. Guidoni, Absolute single-ion thermometry, Phys. Rev. A **99**, 023412 (2019).

[38] J. Roßnagel, K. N. Tolazzi, F. Schmidt-Kaler, and K. Singer, Fast thermometry for trapped ions using dark resonances, New J. Phys. **17**, 045004 (2015).

[39] C. Lisowski, M. Knoop, C. Champenois, G. Hagel, M. Vedel, and F. Vedel, Dark resonances as a probe for the motional state of a single ion, Appl. Phys. B **81**, 5 (2005).

[40] Y. Tao, T. Chen, H. Wang, J. Zhang, T. Zhang, Y. Xie, P. X. Chen, and W. Wu, Mode-resolved thermometry of a trapped ion with deep learning, Phys. Rev. A **109**, 062434 (2024).

[41] K. G. Johnson, B. Neyenhuis, J. Mizrahi, J. D. Wong-Campos, and C. Monroe, Sensing atomic motion from the zero point to room temperature with ultrafast atom interferometry, Phys. Rev. Lett. **115**, 213001 (2015).

[42] E. Kassa, H. Takahashi, C. Christoforou, and M. Keller, Precise positioning of an ion in an integrated Paul

trap-cavity system using radiofrequency signals, J. Mod. Opt. **65**, 520 (2018).

[43] C. Russo, H. G. Barros, A. Stute, F. Dubin, E. S. Phillips, T. Monz, T. E. Northup, C. Becher, T. Salzburger, H. Ritsch *et al.*, Raman spectroscopy of a single ion coupled to a high-finesse cavity, Appl. Phys. B **95**, 205 (2009).

[44] https://doi.org/10.5281/zenodo.15394014